CRC PRESS

IN VIVO OPTICAL IMAGING OF BRAIN FUNCTION

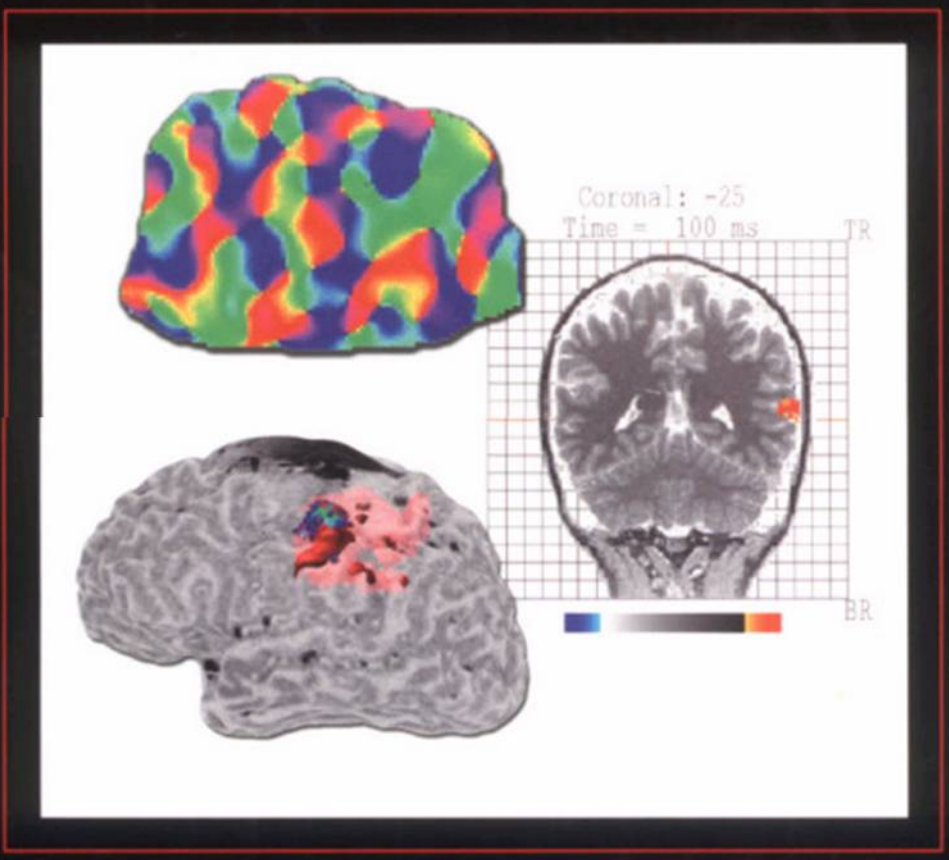

Edited by Ron D. Frostig

METHODS & NEW FRONTIERS IN NEUROSCIENCE

IN VIVO OPTICAL IMAGING OF BRAIN FUNCTION

Edited by
Ron D. Frostig

CRC PRESS

Boca Raton London New York Washington, D.C.

Table of Contents

Chapter 9

Fast Optical Signals: Principles, Methods, and Experimental Results

Gabriele Gratton and Monica Fabiani

1 Voltage-Sensitive and Calcium-Sensitive Dye Imaging of Activity: Examples from the Olfactory Bulb

Michal R. Zochowski, Lawrence B. Cohen, Chun X. Falk, and Matt Wachowiak

CONTENTS

1.1 INTRODUCTION

An optical measurement using voltage-sensitive or calcium-sensitive dyes as indicators of activity can be beneficial in several circumstances. In this chapter we

describe two examples in the study of olfactory processing. In both measurements a large number of neurons or processes are imaged onto each pixel of the camera. Thus, the signals report the average of the changes that occur in this population. For each example we provide some details of the methods used to make the measurements. In addition, because the optical signals are small (fractional intensity changes, $\Delta I/I$, of between 10^{-4} and 5×10^{-2}), optimizing the signal-to-noise ratio in the measurements is important. We will discuss the choice of dyes, sources of noise, light sources, optics, and cameras. The general approach to improving the signal-to-noise ratio is three-pronged. First, test dyes to find the dye with the largest signal-to-noise ratio. Second, reduce the extraneous sources of noise (vibrations, line frequency noise, etc.). Third, maximize the number of photons measured to reduce the relative shot noise (noise arising from the statistical nature of photon emission and detection).

An important advantage of an optical measurement is the ability to make simultaneous measurements from many locations. The two methods described in this chapter also have the advantage of being fast and relatively direct indicators of activity. Both characteristics were important in making maps of the input from receptor neurons and in the study of odor-induced oscillations in the *in vivo* vertebrate olfactory bulb.

Two kinds of cameras have been used in our experiments; both have frame rates faster than 1000 fps. One camera is a photodiode array with 464 pixels and the second is a cooled, back-illuminated, 80×80 pixel CCD camera. Even though the spatial resolution of the two cameras differs rather dramatically, the most important difference is in the range of light intensities over which they provide an optimal signal-to-noise ratio. The CCD camera is optimal at low light levels and the photodiode array is optimal at high light levels.

1.2 CALCIUM- AND VOLTAGE-SENSITIVE DYES

The calcium-sensitive dye used here is thought to be located in the axoplasm and changes the neurons' fluorescence in response to changes in the intracellular free calcium. However, the relationship of the dye signals to calcium concentration is generally nonlinear and the dye response often lags behind the change in calcium. In addition, the dyes add to the calcium buffering in the cytoplasm (Baylor et al., 1983; Neher, 2000). Thus, calcium-sensitive dyes provide a measure for calcium concentration in the axoplasm that must be interpreted with care. Furthermore, in our measurements of the map of the input to the olfactory bulb from olfactory receptor neurons, we are using the calcium signal as a measure of action potential activity in the nerve terminals of the receptor neurons; clearly, this measure is somewhat indirect.

The voltage-sensitive dyes described here are membrane-bound chromophores that change their fluorescence in response to changes in membrane potential. In a model preparation, the giant axon from a squid, these fluorescence signals are fast (following membrane potential with a time constant of <10 μsec) and their size is linearly related to the size of the change in potential (Gupta et al., 1981; Loew et al., 1985). Thus, these dyes provide a direct, fast, and linear measure of the change

in membrane potential of the stained membranes. There are other optical signals from membrane-bound dyes (e.g., absorption and birefringence), and another class of dyes senses membrane potential by redistribution; these topics are discussed elsewhere (Cohen and Salzberg, 1978). Similarly, the evidence that pharmacological effects and photodynamic damage resulting from the voltage-sensitive dyes are manageable can be found in earlier reviews (Cohen and Salzberg, 1978; Salzberg, 1983; Cohen and Lesher, 1986; Grinvald et al., 1988).

Voltage-sensitive and calcium-sensitive dyes might be expected to have signals with differing localization even if they are distributed equally over the area of a neuron. A voltage-sensitive dye is expected to have a signal everywhere a potential change exists: in the cell body, along the axon, and in the nerve terminals. On the other hand, a calcium-sensitive dye is expected to have a signal relatively restricted to the nerve terminal because the calcium influx is largest there. Results consistent with these expectations were obtained by Wachowiak and Cohen (1999).

1.3 MEASURING TECHNOLOGY FOR OPTICAL RECORDINGS

In the two examples presented below, the fractional fluorescence changes ($\Delta F/F$) were small; they ranged from 10^{-4} to 5×10^{-2}. In order to measure these signals, the noise in the measurements had to be an even smaller fraction of the resting intensity. In the sections that follow, some of the considerations necessary to achieve such a low noise are outlined.

1.3.1 Three Kinds of Noise

Shot Noise. The limit of accuracy with which light can be measured is set by the shot noise arising from the statistical nature of photon emission and detection. The root mean square deviation in the number of photons emitted is the square root of the average number emitted (I). As a result, the signal in a light measurement will be proportional to I while the noise in that measurement will be proportional to the square root of I. Thus, the signal-to-noise ratio (S/N) is proportional to the square root of the number of measured photons; more photons measured means a better signal-to-noise ratio.

The basis for this square-root dependence on intensity is illustrated in Figure 1.1. The result of using a random number table to distribute 20 photons into 20 time windows is shown in Figure 1.1A, while Figure 1.1B shows the same procedure used to distribute 200 photons into the same 20 bins. Relative to the average light level, there is more noise in the top trace (20 photons) than in the bottom trace (200 photons). On the right side of Figure 1.1, the measured signal-to-noise ratios are listed and we show that the improvement from A to B is similar to that expected from the above square-root relationship. This square-root relationship holds for all light intensities, as indicated by the dotted line in Figure 1.2, which plots the light intensity divided by the noise in the measurement (S/N) vs. the light intensity. At high light intensities this ratio is large, and thus small changes in intensity can be detected. For example, at 10^{10} photons/msec a fractional intensity change of 0.1%

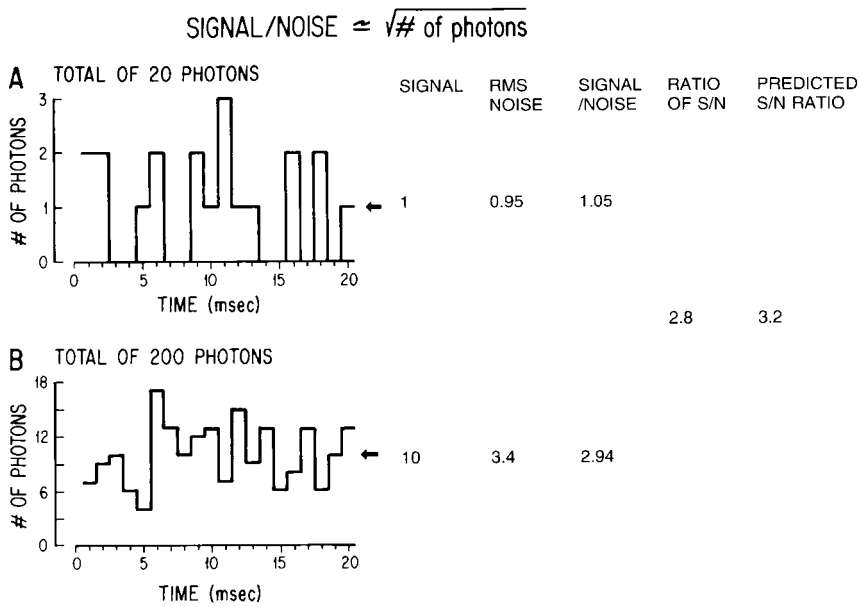

FIGURE 1.1 Plots of the results of using a table of random numbers to distribute 20 photons (top, A) or 200 photons (bottom, B) into 20 time bins. The result illustrates the fact that when more photons are measured, the signal-to-noise ratio is improved. On the right, the signal-to-noise ratio is measured for the two results. The ratio of the two signal-to-noise ratios is 2.8. This is close to the ratio predicted by the relationship that the signal-to-noise ratio is proportional to the square root of the measured intensity. (Redrawn from Wu and Cohen, *Fluorescent and Luminescent Probes for Biological Activity,* Mason, W.T., Ed., Academic Press, London, 1993.)

can be measured with a signal-to-noise ratio of 100. On the other hand, at low intensities the ratio of intensity divided by noise is small and only large signals can be detected. For example, at 10^4 photons/msec the same fractional change of 0.1% can be measured with a signal-to-noise ratio of 1 only after averaging 100 trials. In a shot-noise limited measurement, improvement in the signal-to-noise ratio can be obtained only by 1) increasing the illumination intensity, 2) improving the light-gathering efficiency of the measuring system, or 3) reducing the bandwidth; all of these increase the number of photons in each measurement.

Figure 1.2 compares the performance of two particular camera systems, a photodiode array (solid lines) and a cooled CCD camera (dashed lines) with the shot-noise ideal. The photodiode array approaches the shot-noise limitation over the range of intensities from 3×10^6 to 10^{10} photons/msec. This is the range of intensities obtained in absorption and fluorescence measurements on *in vitro* slices and intact brains in which all of the cells are stained by soaking in a solution of fluorescent dye.

On the other hand, the cooled CCD camera approaches the shot-noise limit over a lower range of intensities, from 3×10^2 to 5×10^6 photons/msec. This is the range of intensities obtained from fluorescence experiments on branches of individual cells and neurons or in experiments where the amount of dye is low. In the discussion

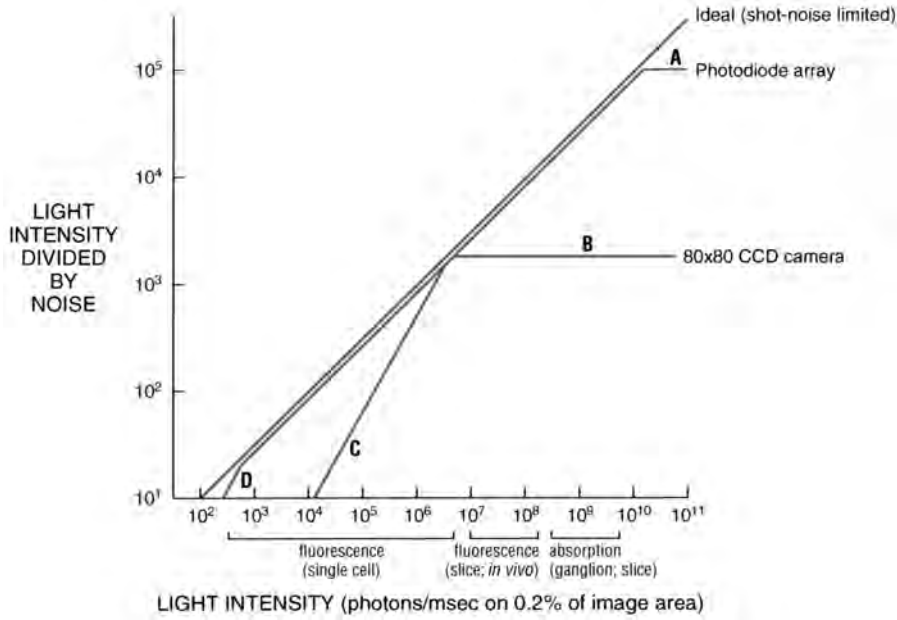

FIGURE 1.2 The ratio of light intensity divided by the noise in the measurement as a function of light intensity in photons/msec/0.2% of the object plane. The theoretical optimum signal-to-noise ratio (dotted line) is the shot-noise limit. Two camera systems are shown, a photodiode array with 464 pixels (solid lines) and a cooled, back-illuminated, 2 kHz frame rate, 80×80 pixel CCD camera (dashed lines). The photodiode array provides an optimal signal-to-noise ratio at higher intensities, while the CCD camera is better at lower intensities. The approximate light intensity per detector in fluorescence measurements from a single neuron, in fluorescence measurements from a slice or *in vivo* preparation, and in absorption measurements from a ganglion or a slice is indicated along the *x* axis. The signal-to-noise ratio for the photodiode array falls away from the ideal at high intensities (A) because of extraneous noise and at low intensities and (C) because of dark noise. The lower dark noise of the cooled CCD allows it to function at the shot-noise limit at lower intensities until read noise dominates (D). The CCD camera saturates at intensities above 5×10^6 photons/msec/0.2% of the object plane (B).

that follows, we will indicate aspects of the measurements and characteristics of the two camera systems that cause them to deviate from the shot-noise ideal. The two camera systems we have chosen to illustrate in Figure 1.2 have relatively excellent dark noise and saturation characteristics. Nonetheless, neither camera is ideal. The photodiode array camera has a limited spatial resolution; while the CCD camera has better spatial resolution, it is saturated at light levels obtained in *in vivo* experiments in which all of the membranes are stained directly with a voltage-sensitive dye.

Extraneous Noise. A second type of noise, termed extraneous or technical noise, is more apparent at high light intensities where sensitivity to this kind of noise is high because the fractional shot noise and dark noise are low. One type of extraneous noise is caused by fluctuations in the output of the light source (see below). Two other sources of extraneous noise are vibrations and movement of the preparation. A number of precautions for reducing vibrational noise have been described (Salzberg

et al., 1977; London et al., 1987). The pneumatic isolation mounts on many vibration isolation tables are more efficient in reducing vertical vibrations than in reducing horizontal movements. One solution is air-filled soft rubber tubes (Newport Corp., Irvine, CA). Minus K Technology sells Biscuit bench-top vibration isolation tables with very low resonant frequencies. They provide outstanding vibration isolation in both planes. Nevertheless, it has been difficult to reduce vibrational noise to less than 10^{-5} of the total light. For this reason, the performance of the photodiode array system is shown reaching a ceiling in Figure 1.2 (segment A, solid line).

Dark Noise. Dark noise will degrade the signal-to-noise ratio at low light levels. Because the CCD camera is cooled and the photosensitive area (and capacitance) is small, its dark noise is substantially lower than that of the photodiode array system. The excess dark noise in photodiode array accounts for the fact that segment C in Figure 1.2 is substantially to the right of segment D.

1.3.2 Light Sources

Three kinds of sources have been used. Tungsten filament lamps are a stable source, but their intensity is relatively low, particularly at wavelengths less than 480 nm. Arc lamps are somewhat less stable but can provide more intense illumination. Opti-Quip, Inc. provides 150- and 250-watt xenon power supplies, lamp housings, and arc lamps with noise in the range of 1 to 3 parts in 10^4. The 150-watt bulb yielded 2 to 3 times more light at 520 ± 45 nm than a tungsten filament bulb and, in turn, the 250-watt bulb was 2 to 3 times brighter than the 150-watt bulb. The extra intensity is especially useful for fluorescence measurements from single neurons or from weakly stained nerve terminals. Measurements made with laser illumination have been substantially noisier (Dainty, 1984).

1.3.3 Optics

Numerical Aperture. The need to maximize the number of measured photons is a dominant factor in the choice of optical components. In the epifluorescence measurements discussed next, both excitation and emitted light pass through the objective, and the intensity reaching the photodetector is proportional to the fourth power of numerical aperture (Inoue, 1986). Therefore, the numerical aperture of the objective is a crucial factor.

Confocal Microscopes. The confocal microscope (Petran and Hadravsky, 1966) substantially reduces scattered and out-of-focus light that contributes to the image. A recent modification using two-photon excitation of the fluorophore further reduces out-of-focus fluorescence and photobleaching (Denk et al., 1995). With both types of microscope, one can obtain images from *in vivo* vertebrate preparations with much better spatial resolution than that achieved with ordinary microscopy. However, at present many milliseconds are required to record the image from a single *x–y* plane. Only with line scans can millisecond temporal resolution be obtained. In addition, the very high Z dimension resolution of confocal microscopy can be a drawback if only a very thin section of the preparation is recorded in each frame. The kinds of problems that can be approached using a confocal microscope are limited by these factors.

1.3.4 CAMERAS

Because the signal-to-noise ratio in a shot noise limited measurement is proportional to the square root of the number of photons converted into photoelectrons (see previous discussion), quantum efficiency is important. Silicon photodiodes have quantum efficiencies approaching the ideal (1.0) at wavelengths where most dyes absorb or emit light (500 to 900 nm). In contrast, only specially chosen vacuum photocathode devices (phototubes, photomultipliers, or image intensifiers) have a quantum efficiency as high as 0.15. Similarly, back-illuminated CCD cameras have a quantum efficiency of >80% at visible wavelengths, while front-illuminated cameras have maximum quantum efficiencies of 20 to 40%.

Many additional factors must be considered in choosing an imaging system. Two important considerations are the requirements for spatial and temporal resolution. Because the signal-to-noise ratio in a shot noise limited measurement is proportional to the square root of the number of measured photons, increases in temporal or spatial resolution will reduce the signal-to-noise ratio. Our discussion considers systems that have frame rates near 1 kHz.

Parallel Readout Arrays. Photodiode arrays with 256 to 1020 elements are now in use in several laboratories (e.g., Iijima et al., 1989; Zecevic et al., 1989; Nakashima et al., 1992; and Hirota et al., 1995). These arrays are designed for parallel readout; each detector is followed by its own amplifier whose output can be digitized at frame rates of 1 kHz. While the need to provide a separate amplifier for each diode element limits the number of pixels in parallel readout systems, it contributes to their very large dynamic range (1 part in 10^5 or 100 db). A discussion of amplifiers has been presented earlier (Wu and Cohen, 1993). Two parallel readout array systems are commercially available: Argus-50 (256 pixels), Hamamatsu Photonics K.K. (www.hpk.co.jp) and NeuroPlex-II (464 pixels), RedShirtImaging LLC (www.redshirtimaging.com).

CCD Cameras. By using a serial readout, the number of amplifiers is greatly reduced. In addition, it is simpler to cool CCD chips to reduce the dark noise. However, because of saturation, CCD cameras presently available do not provide an optimal signal-to-noise ratio for the higher intensities available in some neurobiological experiments (Figure 1.2). This saturation accounts for the bending over of the CCD camera performance at segment B in Figure 1.2. A dynamic range of even 10^3 is not easily achieved with currently available CCD cameras. Thus, these cameras will not be optimal for measurements of absorption or for fluorescence measurements where staining intensity is high. The light intensity would need to be reduced, with a consequent decrease in signal-to-noise ratio. On the other hand, CCD cameras are close to ideal for measurements from branches of individual neurons stained with internally injected dyes. Table 1.1 compares several CCD cameras with frame rates near 1 kHz.

1.4 TWO EXAMPLES

In the experiments described next, we used two basic staining protocols. For the voltage-sensitive dyes, we bathed the turtle olfactory bulb with a solution of the dye for tens of minutes. In contrast, for the calcium-sensitive dye, we infused the

TABLE 1.1
Characteristics of Fast CCD Camera Systems (As Reported by the Manufacturer)

	Frame Rate (Hz) Full Frame	Well Size (×1000 e)	Read Noise (Electrons)	Back Illum.	Bits a to d	Pixels
MiCAM 01[a]	1333	—	—	no	12	92 × 64
Dalsa						
CA-D1-0128[b]	756	300	360	no	12	128 × 128
SciMeasure[c]	2000	300	20 3 @ 100 Hz	yes	14	80 × 80
TILL Photonics						
IMAGO[d]	140	35	14	no	12	160 × 120

[a] www.scimedia.co.jp
[b] www.dalsa.com
[c] www.redshirtimaging.com
[d] www.TILL-photonics.com

dye solution (together with a low concentration of detergent) into the nose of the turtle or mouse and then waited several days for the dye to be transported to the nerve terminals in the olfactory bulb. The choice of dye and the staining procedures are described first in each example. We then show how optical recording of activity in the olfactory bulb can be used to address two different aspects of sensory processing. First we describe the use of calcium-sensitive dyes to determine the map of receptor cell input to the olfactory bulb. Second, we describe the use of voltage-sensitive dyes to study the oscillations that occur in the bulb in response to odor presentation. All of the experimental protocols were approved by the Yale University and the Marine Biological Laboratory Institutional Animal Care and Use Committees.

1.4.1 Maps of Input to the Olfactory Bulb from the Olfactory Receptor Neurons Measured with Calcium-Sensitive Dyes

To understand how odorants are distinguished and to address the question of how an odorant is recognized as the same across a broad concentration range, we measured the spatial pattern of the olfactory receptor neuron input to the olfactory bulb in the three-toed box turtle, *T. triunguis*, and in the C57/Bl6 mouse.

The olfactory receptor axon terminals in the turtle and mouse were selectively labeled by anterograde transport of the dextran-conjugated calcium indicator Calcium Green-1 dextran (10 kD molecular weight; Molecular Probes) applied to the olfactory epithelium using a protocol adapted from Friedrich and Korsching (1997). Turtles were first chilled on ice for 1 to 2 h and then placed upside down with the mouth held open, and 25 to 60 µl of a 2% dye solution dissolved in 0.1 M NaCl plus 0.5% Triton-X 100 was injected into each naris. The pharyngeal opening of

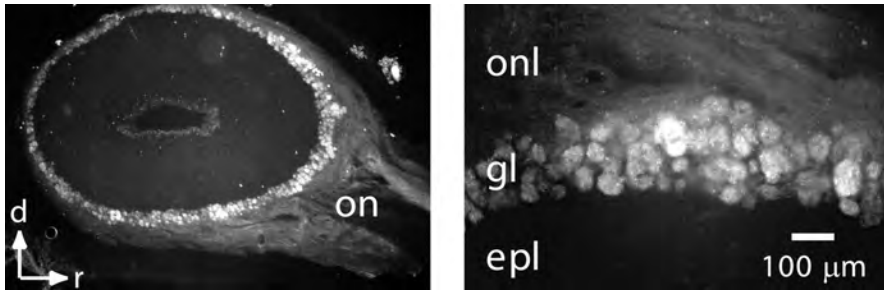

FIGURE 1.3 Calcium Green-1 dextran labeling of turtle olfactory receptor neurons. Sagittal olfactory bulb section showing pattern of dextran labeling. Left: uniform labeling of glomeruli in all olfactory bulb regions. Right: specific labeling of olfactory nerve axons and their terminal branches within glomeruli. Absence of labeling in the external plexiform layer (epl) indicates that the dye is confined to olfactory receptor neurons. Abbreviations: *on*, olfactory nerve; *d*, dorsal; *r*, rostral; *l*, lateral; *onl*, olfactory nerve layer; *gl*, glomerular layer. (M. Wachowiak and L.B. Cohen, unpublished).

each naris was plugged to prevent leakage, and the epithelium was stained for 10 to 20 min, after which the plugs were removed and the mouth closed, allowing the animal to expel the dye from the nose. The turtles were held at room temperature for 4 to 18 days before recording. The nerve terminal labeling was first apparent after about 4 days but appeared most intense after 8 to 10 days. In the nares there was a relatively intense fluorescence in the olfactory cell body layer of the epithelium, while in the olfactory bulb there was a much less intense staining of the olfactory nerve and glomerular layers (Figure 1.3). While glomeruli could be clearly distinguished by the labeled fibers, no fluorescence was visible in subglomerular layers. We observed no differences in the gross appearance of the olfactory epithelium (postmortem examination) or in the size and sensitivity of electroolfactogram (EOG) recordings between stained and unstained animals. Similar methods were used for the mouse and similarly selective staining was obtained.

Because the amount of dye that reaches the nerve terminals is small, the light intensity in such a measurement is low and a better signal-to-noise ratio is obtained with a cooled CCD camera. We formed a magnified (4× or 15×) image of the bulb on an 80×80 CCD camera. For additional details of the methods, see Wachowiak et al. (2001).

We recorded the changes in Calcium Green fluorescence that resulted from a 1- to 2-sec odorant pulse delivered to the nose. In both the turtle and the mouse the signals had approximately the same time course everywhere in the bulb; we therefore characterized the response by the amplitude of the signal as a function of its position on the bulb.

Turtle. We tested several odorants on the same animal. In every instance, the maps were different for different odorants. In some cases a substantial overlap occurred in the activated area, but at higher magnification, the patterns were easily distinguished (data not shown). Thus, the maps of input from the olfactory receptor neurons could be used for odor identification.

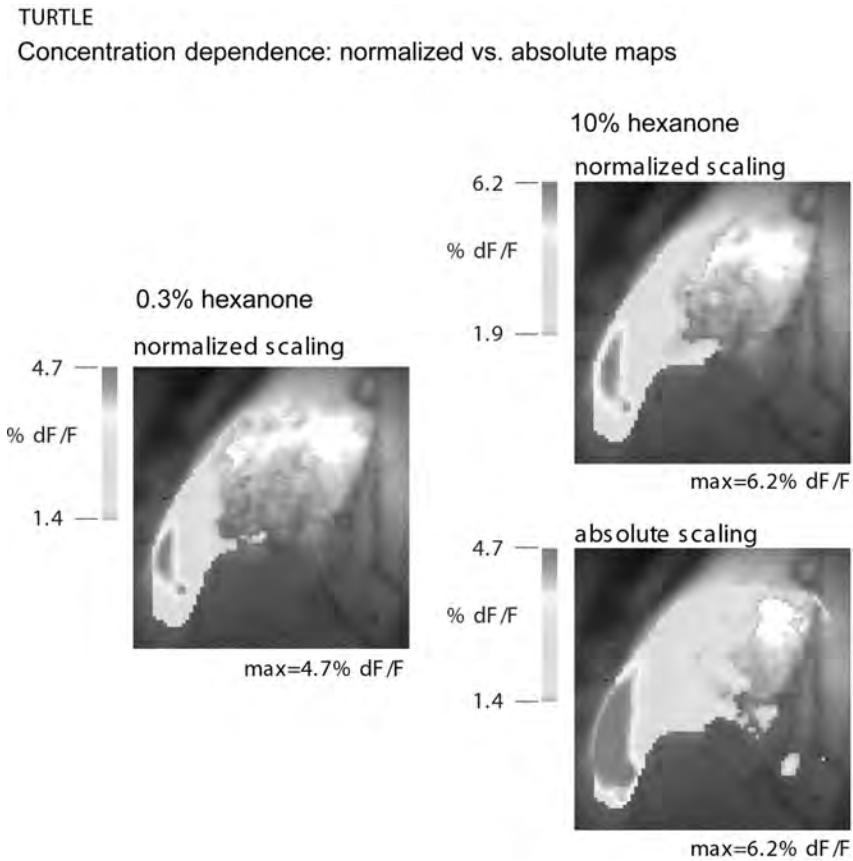

FIGURE 1.4 (See Color Figure 1.4.) Normalized maps of receptor neuron input to the turtle olfactory bulb are concentration-invariant. The left panel shows a pseudocolor map of the response to a 0.3% dilution of saturated vapor of 2-hexanone. The map is normalized to the maximum signal amplitude for this trial. The right panels show pseudocolor maps of a response to a 10% dilution of 2-hexanone. The map on the top is normalized to its maximum signal amplitude. The map on the bottom (absolute scaling) shows the same data using the same scaling as for the 0.3% trial. The figure shows a concentration-dependent increase in the number of glomeruli activated above a given absolute level but shows a concentration invariance in the relative levels of input to all glomeruli activated by an odorant. 4× image magnification. The field of view is approximately 4 × 4 mm.

Color Figure 1.4* shows three pseudocolor representations of activity in response to hexanone at two concentrations in the turtle. Red represents a large signal in each measurement and blue represents a signal 30% as large. The left-hand image shows the response to hexanone at a concentration that was 0.3% of saturation. The largest signal in the response ($\Delta F/F$ = 4.7%) was colored red (normalized scaling). Both right-hand images show the response to 10% hexanone using different

* Color figures follow page 112.

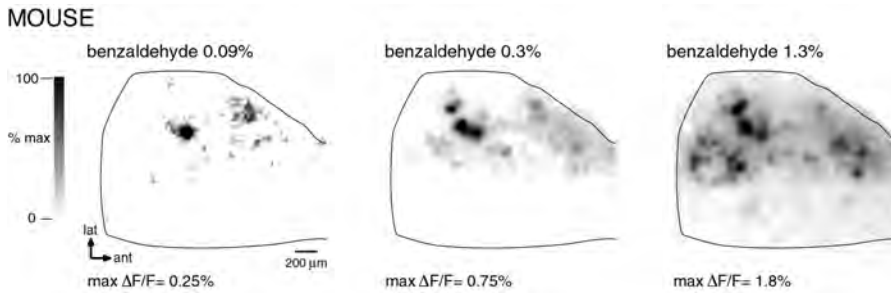

FIGURE 1.5 Normalized maps of receptor neuron input to the mouse olfactory bulb are *not* concentration invariant. The three panels show the normalized response to three concentrations of benzaldehyde. The maps are normalized to the maximum signal amplitude for each measurement.15× image magnification. The field of view is approximately 1 × 1 mm. (M. Wachowiak and L.B. Cohen, unpublished)

scaling procedures. The bottom image shows the response using the same scale as that used for the response to 0.3% hexanone (absolute scaling) where signals of 4.7% and higher are colored red. This image is qualitatively different from the 0.3% image. In contrast, the top image shows the response using normalized scaling; again, the largest signal was colored red. This image is very similar to the image on the left, even though the concentration of odorant differed by a factor of 30. We have observed similar results over a concentration range of up to 600 (data not shown). Thus, normalized maps of input to the turtle olfactory bulb appear to be approximately concentration invariant. We hypothesize that concentration-invariant odorant identification could be achieved if higher olfactory centers "read" the normalized maps of the input to the turtle olfactory bulb.

Mouse. In contrast to the results from the turtle, when similar experiments were carried out in C57/Bl6 mice, the response maps were qualitatively and statistically different at low and high concentrations (Figure 1.5). At low concentrations (<0.3% of saturated vapor) fewer glomeruli were activated by benzaldehyde, while at high concentration more than half of the imaged glomeruli were activated. The reason for the difference in results between turtle and mouse is unclear. The significant concentration-dependent recruitment of input to new glomeruli in the mouse, as compared to the turtle, might reflect differences in the specificity of receptor neurons to a range of odorants, with more broadly tuned receptor neurons showing less recruitment and a higher degree of concentration invariance. It is also unclear whether this apparent difference in the concentration dependence of maps of olfactory bulb input implies that these animals use different strategies for processing olfactory information. One possibility is that the mouse also forms a concentration-invariant map, but at a later stage of olfactory processing.

1.4.2 Oscillations in the Olfactory Bulb in Response to Odors Measured with Voltage-Sensitive Dyes

Choosing Voltage-Sensitive Dyes. Several voltage-sensitive dyes (see, for example, Figure 1.6) have been used to monitor changes in membrane potential in a variety

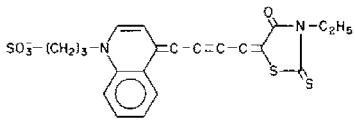

XVII, Merocyanine, Absorption, Birefringence

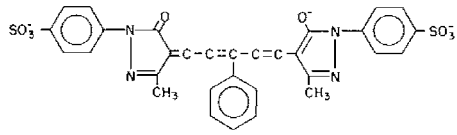

RH155, Oxonol, Absorption

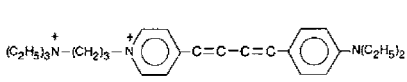

RH414, Styryl, Fluorescence

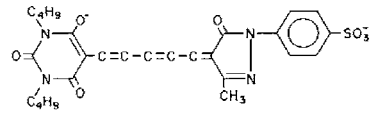

XXV, Oxonol, Fluorescence, Absorption

FIGURE 1.6 Examples of four different chromophores used to monitor membrane potential. The merocyanine dye, XVII (WW375), and the oxonol dye, RH155, are commercially available as NK2495 and NK3041 from Nippon Kankoh–Shikiso Kenkyusho Co. Ltd., Okayama, Japan. The oxonol, XXV (WW781), and styryl, di-4-ANEPPS, are available commercially as dye R-1114 and D-1199 from Molecular Probes, Junction City, OR.

of preparations. This figure illustrates four different chromophores. For each chromophore approximately 100 analogues have been synthesized in an attempt to optimize the signal-to-noise ratio that can be obtained in a variety of preparations. This screening was made possible by synthetic efforts of three laboratories: Jeff Wang, Ravender Gupta, and Alan Waggoner, then at Amherst College; Rina Hildesheim and Amiram Grinvald at the Weizmann Institute; and Joe Wuskell and Leslie Loew at the University of Connecticut Health Center. For each of the four chromophores illustrated in Figure 1.6, there were 10 or 20 dyes that gave approximately the same signal size on squid axons (Gupta et al., 1981). However, dyes that gave nearly identical signals on squid axons gave very different responses on other preparations; thus, tens of dyes usually must be tested to obtain the largest possible signal. Often, dyes that worked well in squid did poorly in other preparations because they did not penetrate through connective tissue or along intercellular spaces to the membrane of interest.

For the *in vivo* measurements of oscillations in the turtle olfactory bulb, the animals were first anesthetized by placing them in ice for 2 h. A craniotomy was performed over the olfactory bulb. The dura and arachnoid matter were then carefully removed to facilitate staining. The exposed olfactory bulb was stained by covering it with dye solution (RH414, 0.02 to 0.2 mg/ml; Grinvald et al., 1994; Molecular Probes, Eugene, OR) for 30 to 60 min. Excess dye was then washed away with turtle saline. In some experiments the dye signals remained stable for several hours. The direct staining with voltage-sensitive dye results in a high light intensity; therefore we used the photodiode array camera (see discussion in Section 1.6). For additional details of the methods, see Lam et al. (1999).

Multiple Components of the Odor-Induced Response. Odor stimuli have long been known to induce stereotyped local field-potential responses consisting of "sinu-

soidal" oscillations of 10 to 80 Hz riding on top of a slow "DC" signal. Since its discovery in the hedgehog (Adrian, 1942), odor-induced oscillations have been seen in phylogenetically distant species including locust (Laurent and Naraghi, 1994), turtle (Beuerman, 1975), and monkey (Hughes and Mazurowski, 1962). Because the optical measurements have a spatial resolution about 25 times better than local field-potential measurements (Zochowski et al., 2000), we obtained a more detailed visualization of the spatio-temporal characteristics of the oscillations.

We found three different oscillations in the bulb in response to odorants. These oscillations differed in amplitude, location, frequency, latency, shape, and duration, but they were similar for the two odorants tested, isoamyl acetate and cineole. In Figure 1.7, the recordings from seven selected diodes in a single trial are shown. The location of these diodes is indicated on the image in the left panel by the

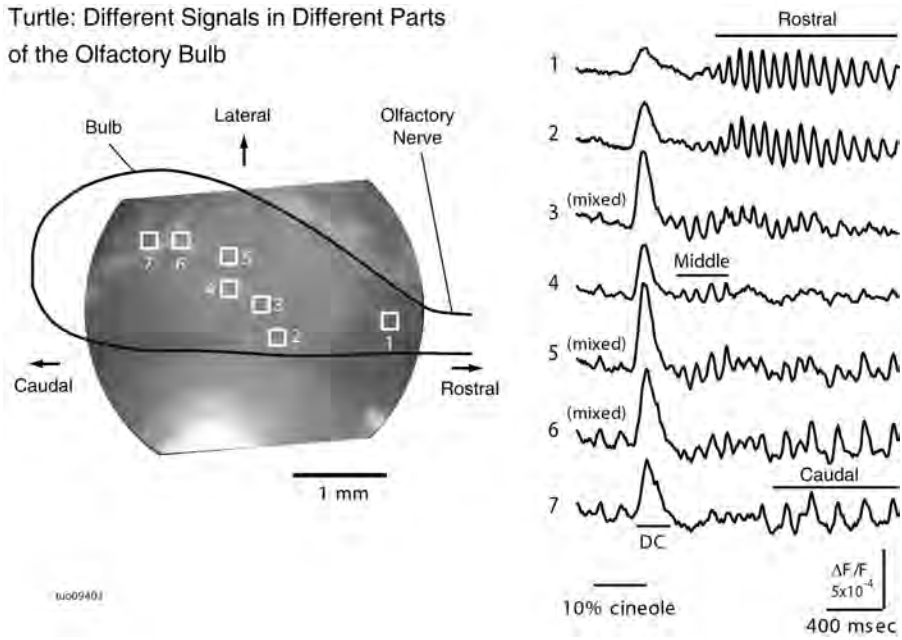

FIGURE 1.7 Simultaneous optical recordings from seven different areas of an olfactory bulb. An image of the olfactory bulb is shown on the left. Signals from seven selected pixels are shown on the right. The positions of these pixels are labeled with squares and numbers on the image of the bulb. All seven signals have a filtered version of the DC signal at the time indicated by the bar labeled DC. The oscillation in the rostral region has a high frequency and relatively long latency and duration (detectors 1 and 2). The oscillation from the middle region has a high frequency and short latency and duration (detector 4). The oscillation from the caudal region has a lower frequency and the longest latency (detector 7). The signal from detectors between these regions (3, 5, and 6) appears to contain a mixture of two components. The horizontal line labeled "10% cineole" indicates the time of the command pulse to the odor solenoid. The data are filtered by a high-pass digital RC (5 Hz) and low-pass Gaussian (30 Hz) filters. (Modified from Lam et al., *J. Neurosci.*, 20: 749, 1999.)

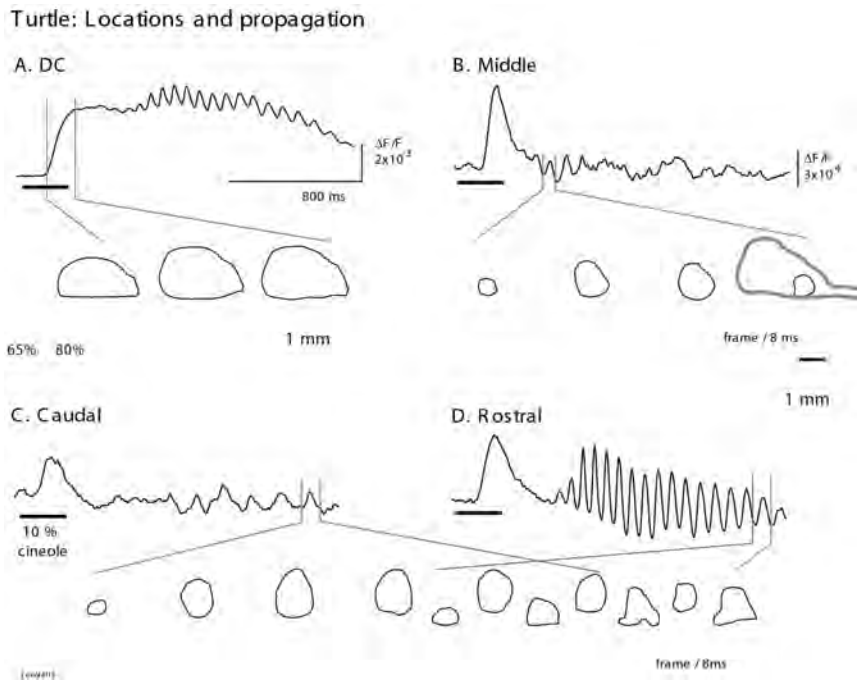

FIGURE 1.8 (See Color Figure 1.8.) The locations and propagation of the four components from the trial shown in Figure 1.7. Multiframe pseudocolor displays of the signals are overlaid on the image of the olfactory bulb. The red color and the black contour lines label the areas where the signals are larger than 80 and 20% of the peak. The DC component in this animal covers almost the entire bulb. The other three panels show the position and propagation of one cycle (indicated by the red and green lines) of the three different oscillations. The black horizontal bars indicate the time of the odor command pulse. The data are filtered by a high-pass digital RC (5 Hz) and low-pass Gaussian (30 Hz) filters. (Modified from Lam et al., *J. Neurosci.*, 20: 749, 1999.)

numbered squares on the left. In rostral locations (detectors 1 and 2), we found a relatively large, long-lasting oscillation with a relatively high frequency (~15 Hz). On a diode from a middle location (detector 4), there was a relatively small, brief, short-latency oscillation (~14 Hz). On detector 7 from the caudal bulb, the oscillation had a lower frequency (~7 Hz) and longer latency. We named the oscillations for the regions of the dorsal bulb in which they occurred: rostral, middle, and caudal. In areas between two regions, the recorded oscillations were combinations of two signals, i.e., rostral/middle in detector 3 and middle/caudal in detectors 5 and 6. The three oscillations also had different shapes — the rostral and caudal oscillations had relatively sharp peaks while the middle oscillation was more sinusoidal.

In addition to the three oscillations, a DC signal, which appears as a single peak after high-pass filtering in Figure 1.7, was observed over most of the ipsilateral olfactory bulb. Color Figure 1.8A shows the time course of an unfiltered recording from the rostral region. Following the start of the odor pulse, the optical signal rose

to a plateau and then continued for a period of seconds. After a delay, the rostral oscillations appeared on the DC response.

Color Figure 1.8 shows the time courses of the signals from four detectors from this trial together with multiple-frame images indicating the position and propagation during one cycle. The rostral, middle, and caudal oscillations are seen more clearly after the DC signal was reduced with a high-pass filter (Color Figure 1.8B, C, D). In these multiframe images, the red color and area enclosed by the black line indicate the areas where the signals are larger than 80 and 20% of the maximum signal. The DC signal covered most of the olfactory bulb. The rostral signal (D) propagated in the caudal direction, the middle signal (B) did not appear to propagate, and the caudal signal (C) propagated in a lateral-caudal direction.

Oscillations are not restricted to the olfactory system. Despite their ubiquity, the roles and functions of oscillation are not well understood. However, in view of their ubiquity and the very large number of neurons that they involve, it is reasonable to speculate that oscillations may have an important role in odor processing. Our data shows that the odor-induced oscillations in the olfactory bulb are substantially more complicated than had been anticipated and that multiple functional population domains are processing olfactory input in parallel.

1.5 NOISE FROM *IN VIVO* PREPARATIONS

Measuring signals from *in vivo* preparations is often more difficult because of noise from the heartbeat and respiration. In the instances described earlier, this kind of noise was not a particular problem because the noise and the signals were at different frequencies and could be separated by frequency filtering. In the turtle the heartbeat and respiration frequencies are about 0.2 Hz, slower than the optical signals, and in the mouse they are about 5 Hz, faster than the signals that we measured. Obviously, this simple solution is not general. Two methods for reducing the movement artifacts from the heartbeat are, together, quite effective. First, a subtraction procedure is used in which two recordings are made but only one of the trials has a stimulus (Orbach et al., 1985). Both recordings are triggered from the upstroke of the electrocardiogram, so both should have similar heartbeat noise. When the trial without the stimulus is subtracted from the trial with the stimulus, the heartbeat artifact is reduced. Second, an airtight chamber is fixed onto the skull surrounding the craniotomy (Blasdel and Salama, 1986). When this chamber is filled with silicon oil and closed, the movements due to heartbeat and respiration are substantially reduced. Using both methods reduces the noise from these movement artifacts enough so that they are no longer the main source of noise in fluorescence measurements.

1.6 FUTURE DIRECTIONS

Because the light-measuring apparatus is already reasonably optimized (see previous discussion), any improvement in sensitivity will need to come from the development of better dyes or investigating signals from additional optical properties of the dyes. The dyes in Figure 1.6 and the vast majority of those synthesized are of the general

class named polyenes (Hamer, 1964). It is possible that improvements in signal size can be obtained with new polyene dyes (see Waggoner and Grinvald (1977) and Fromherz (1991) for a discussion of maximum possible fractional changes in absorption and fluorescence). On the other hand, the fractional change on squid axons has not increased in recent years (Gupta et al., 1981; Cohen et al., unpublished results), and most improvements (e.g., Grinvald et al., 1982; Momose–Sato et al., 1995; Tsau et al., 1996; Antic and Zecevic, 1995) have involved synthesizing analogues that work well on new preparations.

The best of the styryl and oxonol polyene dyes have fluorescence changes of 10 to 20%/100 mv in situations where the staining is specific to the membrane whose potential is changing (Grinvald et al., 1982; Loew et al., 1992; Rohr and Salzberg, 1994). Recently, Gonzalez and Tsien (1995) introduced a new scheme for generating voltage-sensitive signals using two chromophores and energy transfer. While these fractional changes were also in the range of 10%/100 mv, more recent results are about 30% (Gonzalez and Tsien, personal communication). However, because one of the chromophores must be very hydrophobic and does not penetrate into brain tissue, it has not been possible to measure signals with this pair of dyes in intact tissues (Gonzalez and Tsien; Obaid and Salzberg; personal communications). Cacciatore et al. (1999) have used a less hydrophobic oxonol to improve the dye penetration and measured changes in membrane potential in leech neurons during swimming. However, reducing the hydrophobicity also resulted in a substantially slower (~100 msec) response time for the optical signal.

Neuron-Type Specific Staining. An important new direction is the development of methods for neuron-type specific staining. Three quite different approaches have been tried. First, the use of retrograde staining procedures has recently been investigated in the embryonic chick and lamprey spinal cords (Tsau et al., 1996). An identified cell class (motoneurons) was selectively stained. In lamprey experiments, spike signals from individual neurons were sometimes measured (Hickie et al., 1996). Further efforts at optimizing this staining procedure are needed. The second approach is based on the use of cell-type specific staining developed for fluorescein by Nirenberg and Cepko (1993). It might be possible to use similar techniques to selectively stain cells with voltage-sensitive or ion-sensitive dyes. Third, Siegel and Isacoff (1997) constructed a genetically encoded combination of a potassium channel and green fluorescent protein. When introduced into a frog-oocyte, this molecule had a (relatively slow) voltage-dependent signal with a fractional fluorescence change of 5%. More recently, Sakai et al. (2001) and Ataka and Pieribone (2002) have devised GFP-channel constructs with much faster kinetics. Neuron-type specific staining would make it possible to determine the role of specific neuron types in generating the input–output function of a brain region.

Roger Tsien and collaborators have developed a genetically encoded calcium indicator based on fluorescence energy transfer between CFP and YFP bound to calmodulin (Miyawaki et al., 1997). While we are not aware of the use of these molecules in *in vivo* preparations, improvements in the probes (Griesbeck et al., 2001) may improve their utility.